

RESEARCH ARTICLE

10.1002/2015JD024111

Key Points:

- CALIPSO satellite images show gullwing-shaped cirrus above the anvil of some thunderstorms
- Gullwing cirrus indicates an injection of water substance into the stratosphere
- The mechanism responsible for this injection is gravity wave breaking at the storm top

Correspondence to:

P. K. Wang,
pwang1@wisc.edu

Citation:

Wang, P. K., K.-Y. Cheng, M. Setvak, and C.-K. Wang (2016), The origin of the gullwing-shaped cirrus above an Argentinian thunderstorm as seen in CALIPSO images, *J. Geophys. Res. Atmos.*, 121, doi:10.1002/2015JD024111.

Received 19 AUG 2015

Accepted 29 MAR 2016

Accepted article online 4 APR 2016

The origin of the gullwing-shaped cirrus above an Argentinian thunderstorm as seen in CALIPSO images

Pao K. Wang^{1,2}, Kai-Yuan Cheng¹, Martin Setvak³, and Chen-Kang Wang²

¹Department of Atmospheric and Oceanic Sciences, University of Wisconsin-Madison, Madison, Wisconsin, USA,

²Research Center for Environmental Changes, Academia Sinica, Taipei, Taiwan, ³CHMI Satellite Department, Praha 4, Czech Republic

Abstract Gullwing-shaped cirrus layers are observed on an image above a severe thunderstorm occurred in Argentina taken by the instrument CALIOP on board of the CALIPSO satellite. The cirrus layers extended into a level in the stratosphere even higher than the above-anvil cirrus plumes that had been studied previously. This paper utilized the cloud model simulation results of a similar storm to explain the formation of such gullwing cirrus. It is shown that these cirrus layers can form from the moisture transported upward by successive internal gravity wave breaking at levels higher than the above-anvil plumes. The vertical locus of the wave crests where wave breaking occurs is itself gullwing-shaped which is the main reason why the thin cirrus layers are also gullwing shaped. Model results indicate that wave breaking can transport materials irreversibly into higher stratospheric layers and the gullwing-shaped cirrus is an evidence of this transport process.

1. Introduction

The launch of NASA A-Train satellites [L'Ecuyer and Jiang, 2010, <http://atrain.nasa.gov/>] has produced new types of remote sensing data that researchers can use to study the atmosphere. The two special satellites relevant to the present paper are the CloudSat and CALIPSO that provide vertical cross-sectional data in addition to the conventional horizontal view images provided by other satellites. The combination of horizontal and vertical data will be extremely useful in many studies when both are available for the same location and the same time. This is especially so for the study of the atmospheric environment above thunderstorms, the subject of interest in this paper, since direct observation of that region is either impossible or too dangerous to perform.

The instrument used by CloudSat is the 94 GHz *Cloud Profiling Radar* (CPR) whereas that by CALIPSO is the two-wavelength (532 nm and 1064 nm) *Cloud-Aerosol Lidar with Orthogonal Polarization* (CALIOP). The longer wavelength CPR is not capable of detecting smallest ice particles present above the storm, whereas the CALIOP cannot penetrate the optically thick storm top but can detect the optically thin small particles above it. The two instruments thus provide somewhat different information about the cloud tops of the same storm and are complementary to each other. To understand the physics of the region above thunderstorms where small particles of thin concentration are likely to be present, CALIPSO data are usually more directly applicable than CloudSat data. But there are also occasions that CloudSat sees a cloud while CALIPSO does not. This occurs when cloud particles are relatively large, but the concentration is low [Hagihara et al., 2014].

Severe storms tend to excite vigorous cloud top motions that influence the region above the storm and have high potential of impacting the stratosphere, for example, by causing moisture to be transported through the tropopause [see, e.g., Wang, 2003, 2004; Wang et al., 2009, 2011; Iwasaki et al., 2015] causing changes in the water vapor concentration in the lower stratosphere. Deep convective transport of water substance have been observed directly [e.g., Hanisco et al., 2007; Khaykin et al., 2009; Anderson et al., 2012; Homeyer et al., 2014]. Since water vapor is a strong greenhouse gas, the changing vapor concentration in the stratosphere may have significant impact on the global climate [e.g., Pan et al., 1997; Solomon et al., 2010; Uma et al., 2013], and therefore, it is important to understand the physical processes occurring above the storms. CALIPSO data can provide direct information for understanding these processes if correctly interpreted. This paper addresses one of such processes.

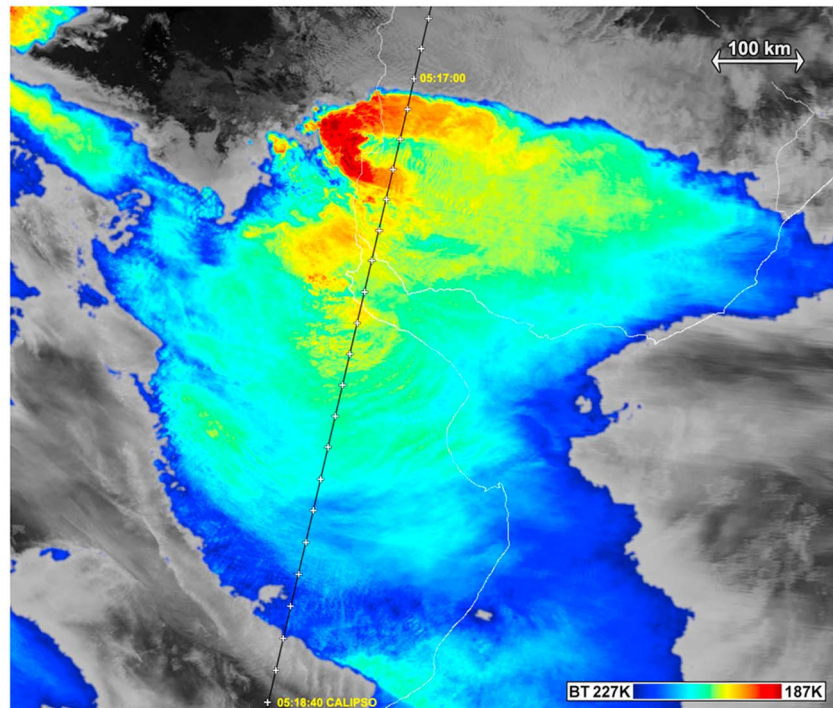


Figure 1. Color-enhanced MODIS band 31 (range of the enhancement: 187 K (dark blue) to 227 K (dark red)) image of 23 December 2009, 05:16 UTC, MODIS/Aqua of convective storms above Argentina and Uruguay (center of the storms about 33S/58W). The black line running from top right to bottom left represents the track of the CALIPSO satellite.

2. Gullwing-Shaped Plumes in CALIPSO Images

Figure 1 shows a storm system which occurred in the Uruguay-Argentina region on 23 December 2009, as captured by MODIS channel 31 image at 05:15:56 UTC. The main storm of interest of this paper is the northernmost one with prominent red “cold-U” signature at the cloud top. This storm has been discussed in greater details in *Setvak et al.* [2013]. Storms with such a signature have high probability of being severe [e.g., *Adler et al.*, 1985]. The apex of the “U” usually indicates the upstream portion of the storm with overshooting top somewhere near the apex [see, e.g., *Heymsfield and Blackmer*, 1988]. The interaction of the ambient wind with the overshooting top causes the anvil of the storm to form the chevron shape. The reason why the U is cold is still being debated but is not the focus of this paper, and we will not discuss it further.

The elongated shape of the anvil of this storm indicates that it has a high wind shear at the storm top level. In an environment of low wind shear, the storm anvil would look more or less circular instead of elongated. The orientation of the cold-U in Figure 1 indicates that the storm-relative wind direction at the storm top level is approximately WNW above this storm. Examples of satellite storm images with high upper level wind shear and relevant discussions can be seen in many previous studies, for example, *Heymsfield and Blackmer* [1988].

The slant black line indicates trajectory of the CALIPSO satellite, while the small crosses along the line are time stamps of the position of the satellite (at 5 s intervals). As can be seen, the CALIPSO passed over the storm system in a track crossing from NNE to SSW over the region somewhat downstream of the coldest part of the cold-U. Between the two arms of the U was a generally warm region. The track is approximately normal to the wind direction.

Figure 2 shows a cross section of the CALIPSO CALIOP 532 nm lidar backscattering coefficient profile obtained along this trajectory. The focus of our study is the gullwing-shaped thin cirrus layer indicated by the white arrows. We shall call such cirrus layer as “gullwing cirrus” in this paper. The first gullwing cirrus (left) labeled “E” seems to rise from an already heightened block of cloud materials, which corresponds to the warmer inner part of the cold-U in Figure 1 [*Setvak et al.*, 2013]. The gullwing cirrus farther south (right) labeled as “H” is smaller and the leveling off is less obvious but still present.

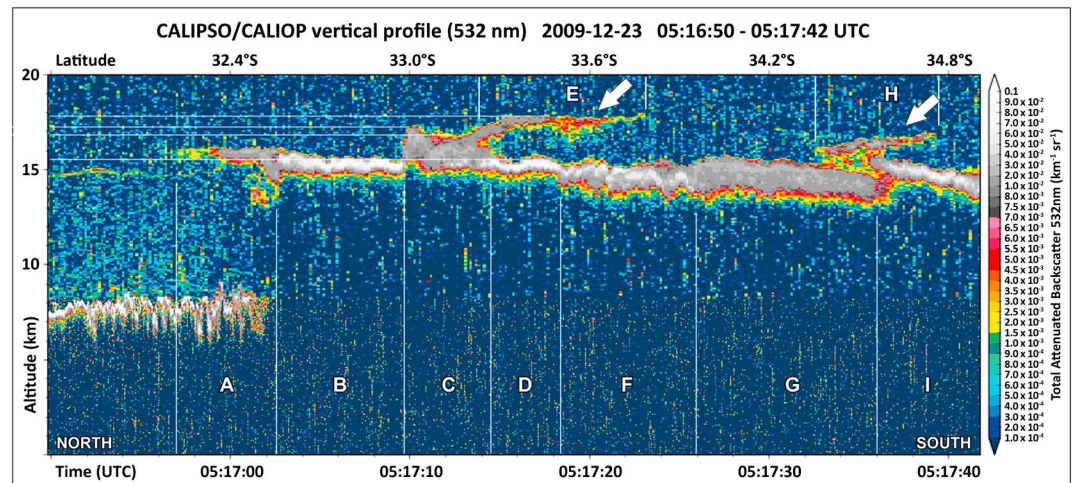


Figure 2. CALIPSO/CALIOP profile of the storm system along the track indicated in Figure 1.

Why would the cirrus layer take the gullwing shape? In order to explain the formation of this gullwing characteristic, we will use cloud model simulation results of a storm of similar type to demonstrate the mechanism that we believe is responsible. In the following, we shall show that the gullwing shape is mainly due to the breaking of the upward propagating internal gravity waves excited by the deep convection of the storm.

The storm we will use for model simulation to demonstrate this feature is the CCOPE (Cooperative Convective Precipitation Experiment) supercell storm occurred on 2 August 1981 in the High Plains in U.S. Midwest. This supercell had been observed extensively and well documented (see *Knight* [1982] for a summary) and modeled by us successfully previously using a cloud model developed by the lead author's research group [Straka, 1989; Johnson *et al.*, 1993, 1994]. The reason to use this particular storm for demonstration is that it was also developed in a highly sheared upper level environment like the one studied here, and indeed, the modeled storm top morphology looks quite similar to the present one. We believe that similar storm environments would produce storms with similar storm top characteristics so that we can select the appropriate sections of the simulated storm top for comparing with the observation.

The fact that we pick a highly sheared storm case for the simulation should not be taken as indicating that internal gravity wave breaking occurs only in such storms or implying that there is always wave breaking in a sheared storm. Internal gravity wave breaking depends on many factors such as the strength of the updraft, the stability of the stratosphere above the storm, the thermodynamic structure of the storm top that leads to the buildup of critical layers, etc. In addition, how much water vapor can be transported by wave breaking depends very much on the details of the microphysics, dynamics, and thermodynamics of the storm environment, which is not the focus of this paper. The main purpose of this paper is to show that a highly sheared storm such as the one shown in Figure 1 can indeed produce the gullwing-shaped cirrus plumes as observed by CALIOP in Figure 2. We believe this will be helpful in the interpretation of the CALIPSO data so that they can be made useful for scientific studies such as the transport of trace chemical species between the troposphere and stratosphere. We do plan to perform systematic studies of the types of storms and their geographical distributions that are conducive to such wave breaking transport in the future.

As indicated previously, we will employ a cloud-resolving model to perform simulations of the CCOPE supercell and analyze the results to explain the physics of the gullwing cirrus. We have run the simulations of the CCOPE storm in various grid resolutions and kept fairly extensive sets of the model results by using a cloud model WISCDYMM developed by P. K. Wang's group (see *Straka* [1989] and *Johnson et al.* [1993, 1994] for the basic setup of the model). WISCDYMM is a single-moment model that it only predicts the mixing ratios of water substances. There are studies showing that single-moment models can lead to substantial errors in predicting hydrometeor physical properties and consequently also thermodynamic and dynamic properties of the cloud [see, e.g., *Igel et al.*, 2015]. In order to minimize possible ambiguities, we use a double-moment model WISCDYMM-II which is also developed recently by Wang's group for simulation in this study. A brief summary of the properties of WISCDYMM-II is given below.

3. Cloud Model WISCDYMM-II

WISCDYMM stands for Wisconsin Dynamic and Microphysical Model which was developed in P. K. Wang's research group in University of Wisconsin-Madison. The earliest form was described in *Straka* [1989] and subsequently modified by others [*Johnson et al.*, 1993, 1994; *Lin and Wang*, 1997]. The new WISCDYMM-II is a newer double-moment model with new dynamics and microphysical parameterizations that we have developed recently, and its properties are briefly described in the following subsections.

WISCDYMM-II is formulated based on a fully compressible nonhydrostatic moisture equation as described by *Klemp et al.* [2007]. It implements a 1.5-order turbulence closure for subgrid eddy mixing and uses Arakawa C-grid and time-split integration for acoustic and gravity wave modes [*Klemp et al.*, 2007], third-order Runge-Kutta time integration [*Wicker and Skamarock*, 2002], fifth-order WENO (Weighted Essentially Nonoscillatory) advection scheme, and sixth-order spatial filter to suppress nonlinear computational instability [*Xue*, 2000].

The cloud microphysics is equipped with a two-moment (mixing ratio and concentration) scheme for five hydrometeor species including cloud drop, raindrop, cloud ice, snow, and graupel/hail using the same parameterizations described by *Morrison et al.* [2009].

For the boundary conditions, it uses open radiative for lateral boundaries, Rayleigh relaxation for the upper boundary, and nonslip condition for the bottom boundary.

We have performed many test runs, and the results are satisfactory. The overall results of dynamics and thermodynamics agree reasonably well with observed storms and also our previous model results using WISCDYMM. But the capability of predicting both mixing ratio and concentration of hydrometeors can reduce the ambiguity in the interpretation of physical processes makes a double-moment model superior to a single-moment model.

Since the main purpose of the present study is to determine whether or not a highly sheared storm such as the CCOPE supercell can produce gullwing cirrus clouds as observed by CALIPSO, we have run both the single-moment WISCDYMM and the double-moment WISCDYMM-II. It turned out that both models produce similar wave breakings in the stratosphere that can transport the moisture upward though the timing, location and magnitude of such events are different. In this paper we will focus on the qualitative question of the plausibility of wave breaking as the responsible mechanism for gullwing cirrus and leave the quantitative question of "how much" to future studies. In the following, the results of WISCDYMM-II will be used for further analysis to illustrate this wave breaking process.

For this study, we ran WISCDYMM-II using a domain of $95 \times 95 \times 95 \text{ km}^3$ with a grid resolution of $0.5 \times 0.5 \times 0.2 \text{ km}^3$. The storm shown in Figure 1 is somewhat larger than the domain size of the simulated storm, but the relevant phenomenon of interest to this study occurred within about 50 km downwind of the overshooting top of the storm; hence, we believe that the current domain size is large enough to illustrate the essential physics of the gullwing cirrus.

Figure 3 shows the simulated storm top temperature field of the simulated CCOPE storm at a randomly chosen time step when the storm has already reached the quasi steady state condition. We use the total hydrometeor mixing ratio $q_{\text{total}} = 0.1 \text{ g/kg}$ surface to represent the cloud top for convenience, but the cloud top temperature pattern looks very similar for 90%, 50%, or 30% RHi (relative humidity with respect to ice) surface, so what is shown in Figure 3 is adequately representative. The cold-U feature occurs at almost every time step of the simulated storm top when the storm reaches quasi steady state, and the major characteristics look the same though details differ from time to time. The colors represent the skin temperature of the cloud top. It is seen that the simulated storm top temperature structure resembles the satellite IR image in Figure 1 in that it contains all the major features such as the cold-U and the warm area downwind and inside the cold-U. This warm area has been called the close in warm area by *Heymsfield and Blackmer* [1988]. The anvil at storm top is elongated downwind by high-level winds just like the one in Figure 1. This indicates that the model physics of WISCDYMM-II produces realistic cloud top temperature field that compares well with observed storm IR features, and hence, it is reasonable to expect that model can produce trustworthy results for simulating storm top physical processes.

The black line on the cloud top in Figure 3 indicates the location where $x = 42.5 \text{ km}$. This line corresponds approximately to the CALIPSO trajectory shown as the black line in Figure 1 in that it runs across both

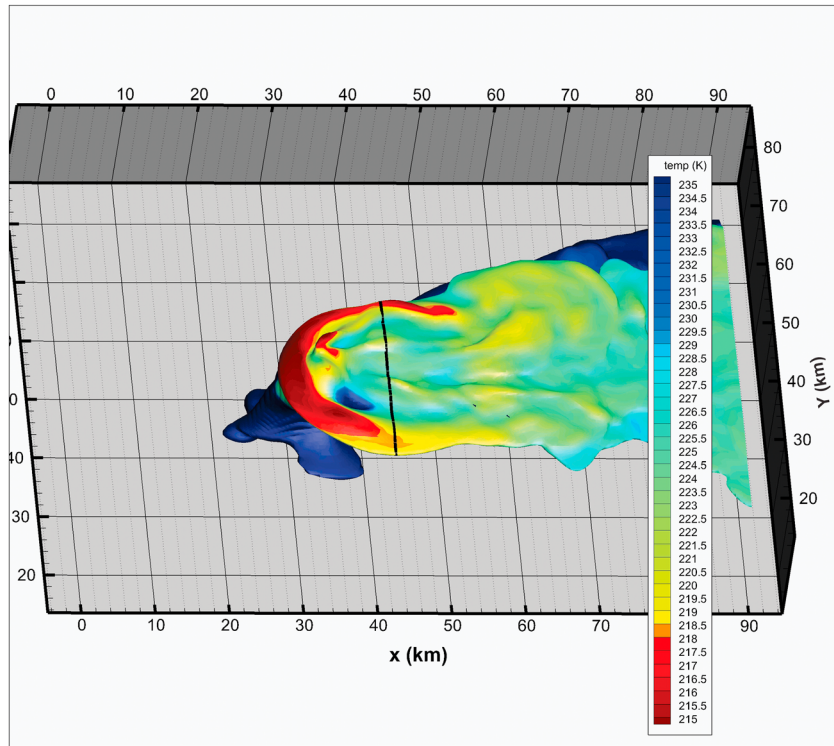


Figure 3. The temperature distribution at the storm top represented by the RHi = 50% isosurface at a randomly chosen time frame. The dashed black line at $x = 42.5$ km denotes the cross section to be shown in Figure 4.

branches of the cold-U and the middle warm area. Given that the thermal features along these two lines are similar, we should expect that the physical processes occurring here should be the same if the model physics is trustworthy. In the following discussions, we will use this cross-sectional view to illustrate the mechanisms generating the gullwing cirrus cloud.

4. Simulated Storm Top Gullwing Features

Figure 4 shows a frame of north-south cross-sectional view of the RHi (relative humidity with respect to ice, in color) field overlaid with black equivalent potential temperature contours at $x = 42.5$ km (same location as indicated by the black line in Figure 3). This cross-sectional view is to approximate the view seen by CALIPSO shown in Figure 2 which was occurring at a similar downwind location relative to the apex of the cold-V. The color scale for RHi is so as to emphasize the moisture features above the storm top which is usually very dry, and the normal color scale would not show these features clearly. We choose RHi field to compare with the CALIOP data shown in Figure 2 because RHi represents the probability of condensation and hence gives good indication where thin cirrus features are likely to be seen by CALIOP. Note that ice may be present even in the very low RHi region in the model results because moisture is averaged out in a grid box of $0.5 \times 0.5 \times 0.2 \text{ km}^3$ in the model calculations, and in reality even in a low RHi grid box, there may be local high RHi pockets that can support the existence of ice crystals (albeit at very low concentration) that are visible to the CALIOP lidar. It is therefore important to focus on the “pattern” of RHi instead of the absolute magnitude of it.

Figure 4 shows that the cloud top is wavy and has many “protrusions.” The wavy shape is caused by the internal gravity waves that are excited by the deep convection and propagate upward. The dark brown protrusions at the storm top bounded roughly between 370 and 380 K in Figure 4 correspond to above-anvil plumes described by *Setvak and Doswell [1991]* and *Levizzani and Setvak [1996]* and explained by *Wang [2003, 2004, 2007]* and *Wang et al. [2011]*. They correspond to the heightened block of cloud materials in Figure 2 mentioned previously. It is further seen that there are moisture streamers (lighter reddish color) stemming upward and outward from the above-anvil plumes. All of these streamers take the gullwing shape,

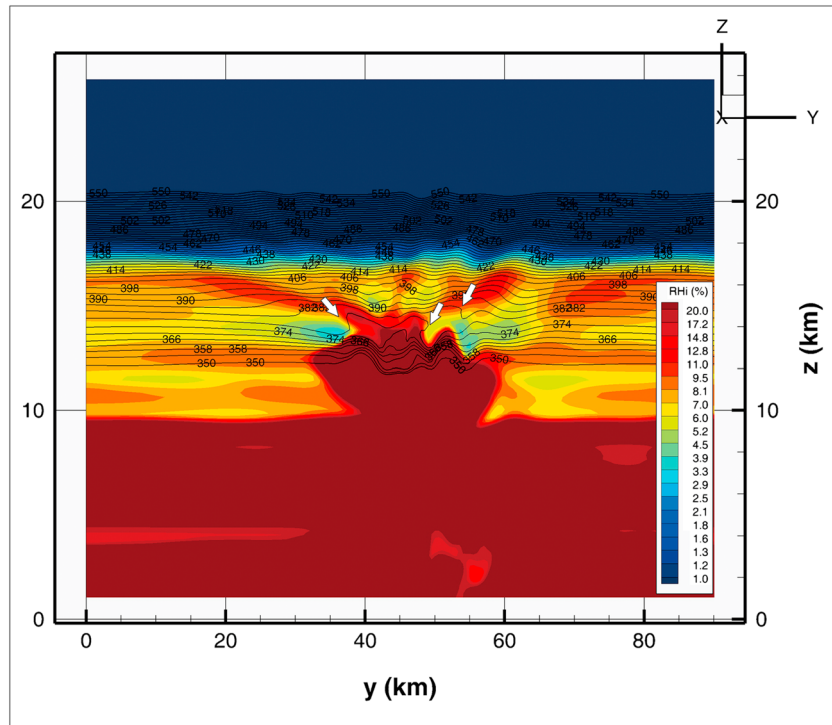


Figure 4. The north-south cross section at $x = 42.5$ km of the RH field at a randomly chosen time frame of the simulated CCOPE supercell showing the gullwing-shaped plumes in the stratosphere. White arrows indicate locations where wave breaking is occurring.

similar to the gullwing cirrus indicated by arrows in Figure 2. This pattern is visible not only in Figure 4 but also in Figure 5 which is the vertical cross section at $x = 50$ km at the same time frame. Furthermore, this feature shows up in all time frames when the simulated storm reaches steady state and therefore is a very common characteristic of the moisture streamers in the above storm region.

As mentioned above, the wavy θ_e contours above the storm manifest the presence of the internal gravity waves in the stratosphere excited by the storm. Closer examination of the moisture streamer indicated by the white arrow in Figure 4 and the θ_e contours reveal that (1) the streamers appear to travel through the θ_e surfaces and (2) the streamer paths are aligned approximately along the locus of wave crests of the gravity waves. These observations can be interpreted as follows.

The fact that the moisture streamers run across the θ_e surfaces indicates that they are transported upward by a *nonadiabatic* process because an adiabatic transport would have the streamer *traveling along*, instead of *intersecting*, the θ_e surfaces. Thus, the streamer intersecting the isentropic surfaces must be due to diabatic process. Since θ_e has included the effect of latent heat released by condensation, this diabatic process cannot be due to pure latent heating. The nature of this noncondensational diabatic process can be understood by examining the observation (2) in the previous paragraph.

Observation (2) says that the streamer paths line approximately along the locus of wave crests, implying that this diabatic process must be associated the wave process near the crest. As we know, normal propagation of gravity waves is an adiabatic process and does not cause mass transfer through the θ_e surface [see, e.g., Holton *et al.*, 1995; Pedlosky, 2003]. However, when wave breaking occurs, materials can be transported through the θ_e surface because wave breaking is an irreversible diabatic process. The wave crest is precisely where wave breaking occurs. Indeed, careful inspection of the θ_e isotherms indicated by the white arrows in Figures 4 and 5 show clear signature of wave breaking. The shape of these isotherms exhibits the characteristics of turning over ocean waves when they arrive on the beach.

The wave breakings in Figures 4 and 5 occur at $z \sim 14$ km whereas the observed tropopause of the CCOPE supercell is at $z \sim 12.5$ km [see Johnson *et al.*, 1993], thus, the breaking clearly occurs in the stratosphere.

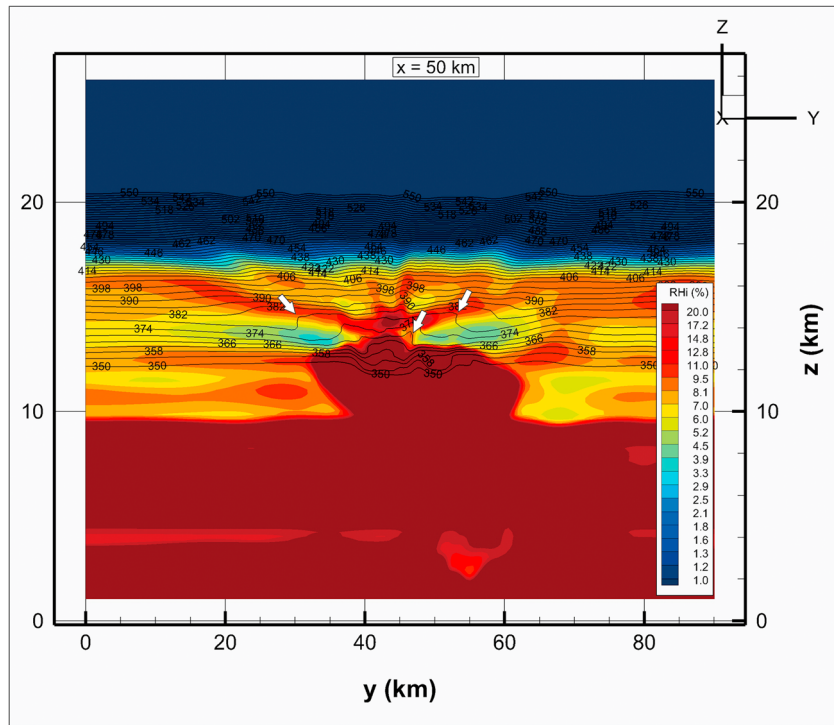


Figure 5. The north-south cross section at $x = 50$ km of the RHi field at the same time frame as Figure 4 of the simulated CCOPE supercell showing similar gullwing-shaped plumes in the stratosphere. White arrows indicate locations where wave breaking is occurring.

Examining the model output reveals that wave breaking can occur at an altitude as high as 16 km, indicating that this mechanism can transport moisture well into the lower stratosphere.

The shape of the wave breaking θ_e isotherms implies that there are vicinity areas where the vertical gradient of θ_e is negative under the crest, i.e., $\frac{\partial \theta_e}{\partial z} < 0$. This means that the wave breaking region is characterized by this negative gradient, and we can use this criterion to examine where wave breaking is occurring in the vicinity of a storm. We shall only focus on the region above the tropopause in this study. Figure 6 shows the negative $\frac{\partial \theta_e}{\partial z}$ areas near the 378 K isotherm (the one indicated by the leftmost white arrow in Figure 5).

Figure 7 shows a x - y view of the regions (blue isosurface) where $\frac{\partial \theta_e}{\partial z} = 0$ inside which the vertical θ_e gradient is negative. These blue isosurfaces indicate where wave breaking occurs. It is seen here that the breaking region above the anvil forms a two-wing structure, more or less like the wake of a ship moving on still water. This pattern of breaking regions remains more or less persistent throughout the 2 h simulation period though the intensity varies significantly. The locations of breaking regions also vary but are always near the storm top.

Figure 8 shows the x - z (east-west) view of the wave breaking locations. We see that the region immediately downwind of the overshooting top is a place where wave breaking occurs vigorously. The general highest altitude of breaking is around 15 km. In some other time frames, the breaking region can be as high as 16 km. This occurs usually near the region above the overshooting top. We plan to make a more detailed study on the evolution of the wave breaking regions and report the results in the future.

Thus, as the gravity waves propagate upward and outward from the storm top, the wave breaking at the crests allows moisture (either water vapor or possibly small ice crystals) to be transported irreversibly through the isentropic surfaces to higher levels. Such wave breaking above the storm top has also been demonstrated in Wang [2003, 2004, 2007] also using cloud model simulations.

For a simple upward propagating gravity wave in an environment of no wind shear, the loci of all points of constant phase are circular cones [see, e.g., Pedlosky, 2003]. In the presence of wind shear, the constant phase surfaces become more complicated but still close to quasi-circular cones each similar to a table top soup

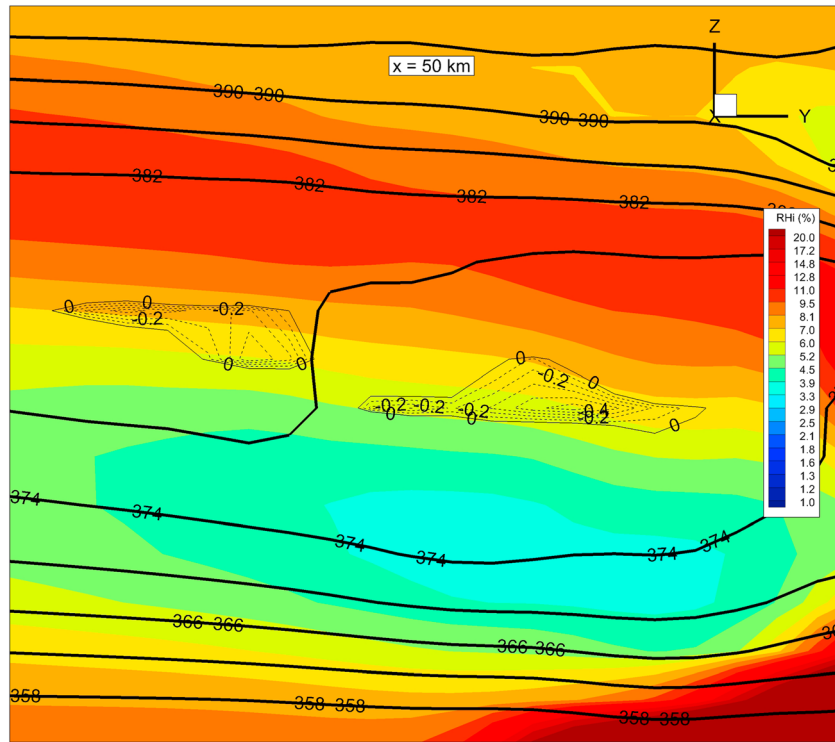


Figure 6. Distribution of (thin black contours, negatives are dashed) in the vicinity of the breaking isotherm 378 K indicated by the left white arrow in Figure 5. Only the negative gradient regions are shown. Thick black contours are equivalent potential temperature and colors are RHi (same scale as in Figure 5).

plate. As the wave propagates to upper levels, the cone expands outward. The intersection of this cone with a vertical cross section is a curve roughly like a wide-open alphabet “V” as we see in Figure 4. This is to say that a locus of wave crests on the vertical cross section is also of V shape. But the slope of the locus can change with height, either becomes steeper or more horizontal, depending on local stratification (i.e., stability) of the stratosphere [Pedlosky, 2003]. At very high levels the angle usually becomes more horizontal as the wave energy is more dissipated already. The net effect is that a moisture streamer that is transported by the successive breaking wave crests forms a vertical profile that resembles a gullwing when observed by the vertically slicing CALIOP as seen in Figure 2.

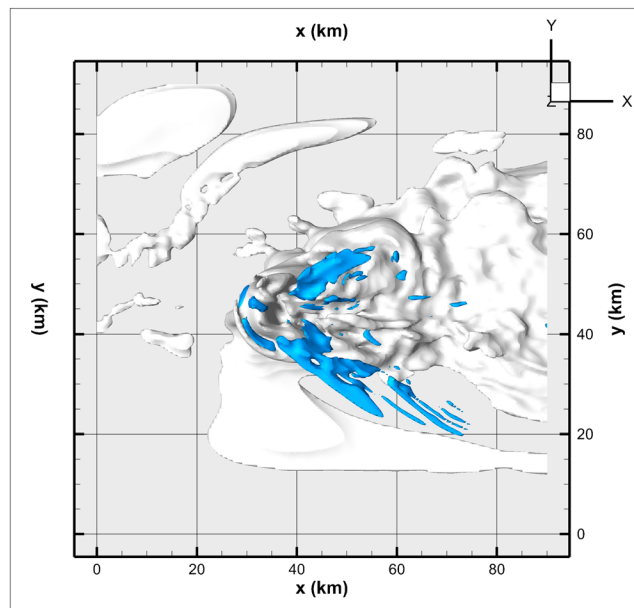


Figure 7. Top (x-y) view of the simulated CCOPE storm at the same time frame as in Figure 4 showing the regions where $\frac{\partial w}{\partial z} \leq 0$ (blue). The gray color represents the RH = 80% isosurfaces used to represent the approximate cloud boundaries.

Note that the lining up of a moisture streamer with vertical crest locus is not exact but only approximate as the locus is formed by joining the wave crests at a specific instance whereas the streamer trajectory has included the effects of time it takes to transport upward, wind, and local turbulent mixing (and these have all been taken into account by the

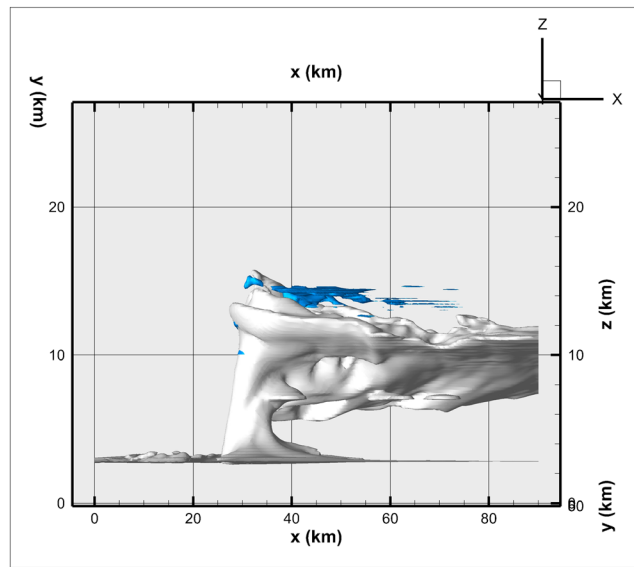


Figure 8. East-west (x - z) view of the simulated CCOPE storm at the same time frame as in Figure 4 showing the regions where $\frac{\partial RH}{\partial z} \leq 0$ (blue). The gray color represents the RHI = 80% isosurfaces used to represent the approximate cloud boundaries.

model), and hence, the two cannot coincide exactly. Nevertheless, the resulting streamer profile still resembles that of a gullwing.

5. Conclusions

In the above, we have identified a gullwing-shaped thin cirrus layer in lower stratospheric region above a thunderstorm which occurred in Argentina, as seen in CALIPSO CALIOP image. By analyzing the numerical simulation results of a similar storm, we showed that the gullwing cirrus must be produced by the moisture carried upward by a transport process associated with gravity wave breaking. The locus of wave crests where the breaking occurs resembles a gullwing.

The gullwing cirrus layers in Figure 2 appear as the higher branches of the above-anvil plumes reported by *Setvak and Doswell* [1991] and *Levizzani and Setvak* [1996] and explained by *Wang* [2003]. The above-anvil plumes are produced by the “primary” wave breaking right at the storm top that transports substantial amount of water substance whose concentration is large enough to be detected by the 94 GHz CPR. In contrast, the gullwing cirrus layers consist of the smaller amount of moisture coming out of the above-anvil plumes that are transported farther upward due to wave breaking (the “secondary wave breaking”) at higher levels. Their ice concentration is usually too low as to elude the CPR but is ultimately captured by the CALIOP together with the above-anvil plumes.

The presence of gullwing-shaped cirrus is evidence that storm materials can be transported into the stratosphere via the gravity wave breaking process to levels much higher than previously thought. Given the important role played by water substance in the stratosphere, it is clearly of some importance to investigate this process further. It is highly likely that other trace chemicals (both trace gases and aerosol particles) of tropospheric origin can also be transported this way.

This also indicates that it is important to make a global survey of the geographical distributions and the time variations of internal gravity waves propagation caused by deep convection. *Jiang et al.* [2004] had made a survey of tropical deep convective storms and the propagation of gravity waves caused by them using the data from the Upper Atmospheric Research Satellite (UARS) Microwave Limb Sounder. With the understanding of the wave breaking mechanism as described in the present study, one can use their results in conjunction with CALIOP data to make further progress on the research of stratosphere/troposphere exchange process.

References

- Adler, R. F., and R. A. Mack (1986), Thunderstorm cloud top dynamics as inferred from satellite observations and a cloud top parcel model, *J. Atmos. Sci.*, *43*, 1945–196.
- Adler, R. F., M. J. Markus, and D. D. Fenn (1985), Detection of severe Midwest thunderstorms using geosynchronous satellite, data, *Mon. Weather Rev.*, *113*, 769–781, doi:10.1175/1520-0493(1985)113<0769:DOSMTU>2.0.CO;2.
- Anderson, J. G., D. M. Wilmoth, J. B. Smith, and D. S. Sayres (2012), UV dosage levels in summer: Increased risk of ozone loss from convectively injected water vapor, *Science*, *337*(6096), 835–839, doi:10.1126/science.1222978.
- Hagihara, Y., H. Okamoto, and Z. J. Luo (2014), Joint analysis of cloud-top heights from CloudSat and CALIPSO: New insights into cloud top microphysics, *J. Geophys. Res. Atmos.*, *119*, 4087–4106, doi:10.1002/2013JD020919.
- Hanisco, T. F., et al. (2007), Observations of deep convective influence on stratospheric water vapor and its isotopic composition, *Geophys. Res. Lett.*, *34*, L04814, doi:10.1029/2006GL027899.
- Heymsfield, G. M., and R. H. Blackmer (1988), Satellite-observed characteristics of Midwest severe thunderstorm anvils, *Mon. Weather Rev.*, *116*, 2200–2224.

Acknowledgments

This study is partially supported by NOAA GOES-R Risk Reduction Award NA10NES4400013, National Science Foundation grant AGS-1219586, and research support from Academia Sinica and Ministry of Science and Technology, Taiwan. Any opinions, findings, and conclusions or recommendations expressed in this material are those of the authors and do not necessarily reflect the views of the National Science Foundation (NSF). Aqua MODIS Level 1B data were acquired from the NASA Level 1 and Atmosphere Archive and Distribution System (LAADS, <http://ladsweb.nascom.nasa.gov/>); the CALIOP backscatter data used in this paper were acquired from the NASA Langley Research Center Atmospheric Science Data Center (<http://eosweb.larc.nasa.gov/>) archive and visualized using the ENVI and CCPLLOT software.

- Holton, J. R., P. H. Haynes, M. E. McIntyre, A. R. Douglass, R. B. Rood, and L. Pfister (1995), Stratospheric-tropospheric exchange, *Rev. Geophys.*, *33*, 403–439, doi:10.1029/95RG02097.
- Homeyer, C. R., et al. (2014), Convective transport of water vapor into the lower stratosphere observed during double-tropopause events, *J. Geophys. Res. Atmos.*, *119*, 10,941–10,958, doi:10.1002/2014JD021485.
- Igel, A. L., M. R. Igel, and S. C. van den Heever (2015), Make it a double? Sobering results from simulations using single-moment microphysics schemes, *J. Atmos. Sci.*, *72*, 910–925, doi:10.1175/JAS-D-14-0107.1.
- Iwasaki, S., Z. J. Luo, H. Kubota, T. Shibata, H. Okamoto, and H. Ishimoto (2015), Characteristics of cirrus clouds in the tropical lower stratosphere, *Atmos. Res.*, *164–165*, 358–368, doi:10.1016/j.atmosres.2015.06.009.
- Jiang, J. H., B. Wang, K. Goya, K. Hocke, S. D. Eckermann, J. Ma, D. L. Wu, and W. G. Read (2004), Geographical distribution and interseasonal variability of tropical deep convection: UARS MLS observations and analyses, *J. Geophys. Res.*, *109*, D03111, doi:10.1029/2003JD0003756.
- Johnson, D. E., P. K. Wang, and J. M. Straka (1993), Numerical simulation of the 2 August 1981 CCOPE supercell storm with and without ice microphysics, *J. Appl. Meteorol.*, *32*, 745–759.
- Johnson, D. E., P. K. Wang, and J. M. Straka (1994), A study of microphysical processes in the 2 August 1981 CCOPE supercell storm, *Atmos. Res.*, *33*, 93–123.
- Khaykin, S., J.-P. Pommereau, L. Korshunov, V. Yushkov, J. Nielsen, N. Larsen, T. Christensen, A. Garnier, A. Lukyanov, and E. William (2009), Hydration of the lower stratosphere by ice crystal geysers over land convective systems, *Atmos. Chem. Phys.*, *9*, 2275–2287.
- Klemp, J. B., W. C. Skamarock, and J. Dudhia (2007), Conservative split-explicit time integration methods for the compressible nonhydrostatic equations, *Mon. Weather Rev.*, *135*, 2897–2913, doi:10.1175/MWR3440.1.
- Knight, C. A. (1982), The Cooperative Convective Precipitation Experiment [CCOPE], 18 May–7 August 1981, *Bull. Am. Meteorol. Soc.*, *63*, 386–398.
- L'Ecuyer, T. S., and J. H. Jiang (2010), Touring the atmosphere aboard the A-Train, *Phys. Today*, *63*(7), 36–41, doi:10.1063/1.3463626.
- Levizzani, V., and M. Setvak (1996), Multispectral, high resolution satellite observations of plumes on top of convective storms, *J. Atmos. Sci.*, *53*, 361–369.
- Lin, H.-M., and P. K. Wang (1997), A numerical study of microphysical processes in the 21 June 1991 Northern Taiwan mesoscale precipitation system, *Terres. Atmos. Oceanic Sci.*, *8*, 385–404.
- Morrison, H., G. Thompson, and V. Tatarskii (2009), Impact of cloud microphysics on the development of trailing stratiform precipitation in a simulated squall line: Comparison of one- and two-moment schemes, *Mon. Weather Rev.*, *137*, 991–1007, doi:10.1175/2008MWR2556.1.
- Pan, L., S. Solomon, W. Randel, J.-F. Larmarque, P. Hess, J. Gille, E. Chiou, and M. P. McCormick (1997), Hemispheric symmetries and seasonal variations of the lowermost stratospheric water vapor and ozone derived from SAGE II data, *J. Geophys. Res.*, *102*, 28,177–28,184, doi:10.1029/97JD02778.
- Pedlosky, J. (2003), *Waves in the Ocean and Atmosphere: Introduction to Wave Dynamics*, 260 pp., Springer, New York.
- Setvak, M., and C. A. Doswell III (1991), The AVHRR channel 3 cloud top reflectivity of convective storms, *Mon. Weather Rev.*, *119*, 841–847.
- Setvak, M., K. Bedka, D. T. Lindsey, A. Sokol, Z. Charvát, J. Štáštka, and P. K. Wang (2013), A-Train observations of deep convective storm tops, *Atmos. Res.*, *123*, 229–248.
- Solomon, S., K. Rosenlof, R. Portmann, J. Daniel, S. Davis, T. Sanford, and G. Plattner (2010), Contributions of stratospheric water vapor to decadal changes in the rate of global warming. [Available at [www.sciencexpress.org/28 January 2010/10.1126/science.1182488](http://www.sciencexpress.org/28%20January%202010/10.1126/science.1182488).]
- Straka, J. M. (1989), Hail growth in a highly glaciated central High Plains multi-cellular hailstorm, PhD dissertation, 413 pp., Dep. Meteorology, Univ. of Wisconsin, Madison.
- Uma, K. N., S. K. Das, S. S. Das, and K. K. Kumar (2013), Aura-MLS observations of water vapor entering the stratosphere over the northern Bay of Bengal and east equatorial Indian Ocean, *Terr. Atmos. Ocean. Sci.*, *24*, 357–368, doi:10.3319/TAO.2012.11.06.01(A)(2013).
- Wang, P. K. (2003), Moisture plumes above thunderstorm anvils and their contributions to cross tropopause transport of water vapor in midlatitudes, *J. Geophys. Res.*, *108*(D6), 4194, doi:10.1029/2003JD002581.
- Wang, P. K. (2004), A cloud model interpretation of jumping cirrus above storm top, *Geophys. Res. Lett.*, *31*, L18106, doi:10.1029/2004GL020787.
- Wang, P. K. (2007), The thermodynamic structure atop a penetrating convective thunderstorm, *Atmos. Res.*, *83*, 254–262.
- Wang, P. K., M. Setvak, W. Lyons, W. Schmid, and H. Lin (2009), Further evidence of deep convective vertical transport of water vapor through the tropopause, *Atmos. Res.*, *94*, 400–408.
- Wang, P. K., S.-H. Su, Z. Charvat, J. Stastka, and H. M. Lin (2011), Cross tropopause transport of water by mid-latitude deep convective storms: A review, *Terr. Atmos. Ocean. Sci.*, *22*, 447–462.
- Wicker, L. J., and W. C. Skamarock (2002), Time-splitting methods for elastic models using forward time schemes, *Mon. Weather Rev.*, *130*, 2088–2097, doi:10.1175/1520-0493(2002)130<2088:TSMFEM>2.0.CO;2.
- Xue, M. (2000), High-order monotonic numerical diffusion and smoothing, *Mon. Weather Rev.*, *128*, 2853–2864, doi:10.1175/1520-0493(2000)128<2853:HOMNDA>2.0.CO;2.